

RESEARCH ARTICLE | MARCH 28 2024

Structural dynamics around a hydrogen bond: Investigating the effect of hydrogen bond strengths on the excited state dynamics of carboxylic acid dimers

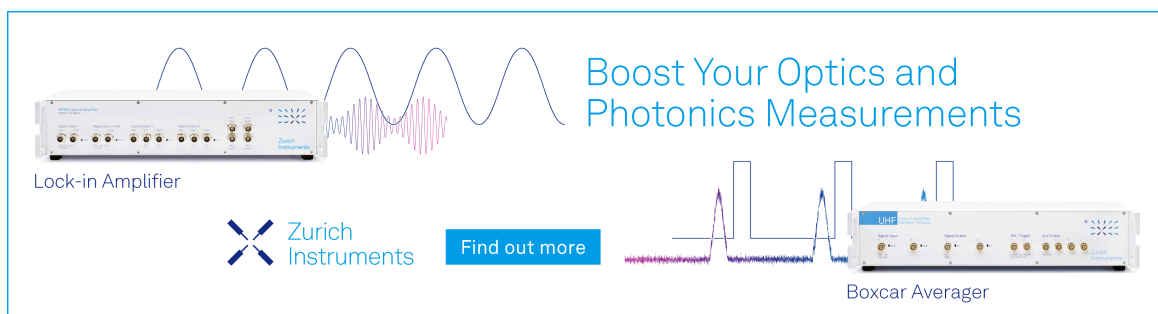
Special Collection: [Time-resolved Vibrational Spectroscopy](#)

E. Plackett ; C. Robertson ; A. De Matos Loja ; H. McGhee ; G. Karras ; I. V. Sazanovich ; R. A. Ingle ; M. J. Paterson ; R. S. Minns  



J. Chem. Phys. 160, 124311 (2024)

<https://doi.org/10.1063/5.0192407>



Boost Your Optics and Photonics Measurements

Lock-in Amplifier

Zurich Instruments

Find out more

Boxcar Averager

Structural dynamics around a hydrogen bond: Investigating the effect of hydrogen bond strengths on the excited state dynamics of carboxylic acid dimers

Cite as: J. Chem. Phys. 160, 124311 (2024); doi: 10.1063/5.0192407

Submitted: 19 December 2023 • Accepted: 12 March 2024 •

Published Online: 28 March 2024



View Online



Export Citation



CrossMark

E. Plackett,¹  C. Robertson,²  A. De Matos Loja,²  H. McGhee,³  G. Karras,⁴  I. V. Sazanovich,⁴ 
R. A. Ingle,³  M. J. Paterson,²  and R. S. Minns^{1,a)} 

AFFILIATIONS

¹School of Chemistry, University of Southampton, Highfield, Southampton SO17 1BJ, United Kingdom

²Institute of Chemical Sciences, Heriot-Watt University, Edinburgh, United Kingdom

³School of Chemistry, University College London, London, United Kingdom

⁴Central Laser Facility, Rutherford Appleton Laboratories, Harwell Campus, United Kingdom

Note: This paper is part of the JCP Special Topic on Time-resolved Vibrational Spectroscopy 2023.

^{a)}Author to whom correspondence should be addressed: r.s.minns@soton.ac.uk

ABSTRACT

The photochemical dynamics of the acetic acid and trifluoro-acetic acid dimers in hexane are studied using time-resolved infrared absorption spectroscopy and *ab initio* electronic structure calculations. The different hydrogen bond strengths of the two systems lead to changes in the character of the accessed excited states and in the timescales of the initial structural rearrangement that define the early time dynamics following UV excitation. The much stronger hydrogen bonding in the acetic acid dimer stabilizes the system against dissociation. Ground state recovery is mediated by a structural buckling around the hydrogen bond itself with no evidence for excited state proton transfer processes that are usually considered to drive ultrafast relaxation processes in hydrogen bonded systems. The buckling of the ring leads to relaxation through two conical intersections and the eventual reformation of the electronic and vibrational ground states on a few picosecond timescale. In trifluoro-acetic acid, the weaker hydrogen bonding interaction means that the dimer dissociates under similar irradiation conditions. The surrounding solvent cage restricts the full separation of the monomer components, meaning that the dimer is reformed and returns to the ground state structure via a similar buckled structure but over a much longer, ~100 ps, timescale.

© 2024 Author(s). All article content, except where otherwise noted, is licensed under a Creative Commons Attribution (CC BY) license (<https://creativecommons.org/licenses/by/4.0/>). <https://doi.org/10.1063/5.0192407>

I. INTRODUCTION

Hydrogen bonds play a critical role in defining the structure and function of molecular systems in their electronic ground state. The role of hydrogen bonds in defining photochemical outcomes is equally important but less understood.^{1–10} Subtle changes to weak non-covalent interactions of the molecule cause significant changes to the photochemical dynamics of the system. For example, the addition of a single hydrogen bond can completely switch off the dominant photochemical processes in an isolated molecule,

reducing it to an insignificant contribution in a molecule bound to another by a hydrogen bond. In previous work on the UV photochemistry of the ammonia dimer in the gas phase, hydrogen transfer between the two ammonia molecules was seen to effectively stabilize the system against the N–H bond dissociation seen in the monomer under the same irradiation conditions.⁷ The hydrogen bond, therefore, opens an alternative reaction pathway that, in this case, is localized on the hydrogen bond itself. The strength of the effect of a hydrogen bond across a wide range of photochemical systems^{7–10} is, perhaps, surprising given the relatively weak nature

of a typical hydrogen bond when compared to covalent bonds or UV photon energies. Despite this importance, our understanding of the relative efficacy of specific hydrogen bond structures or the effect of the hydrogen bond strength on the ensuing dynamics remains rather limited. Here, we report a combined computational and time-resolved infrared (TRIR) absorption experimental study of the photochemistry of two hydrogen bonded acid dimers, acetic acid (AA) and trifluoro-acetic acid (TFA). The structural similarity of the two acids allows us to explore how changes in the strength of the hydrogen bond affect the excited state processes.

A wide range of experimental techniques (photoelectron spectroscopy, transient absorption in both the infrared and visible, etc.), in both the gas and solution phases, have been used to explore the effects of hydrogen bonding on photochemical processes.^{1–8,11–13} Many of these studies have highlighted the importance of excited state proton transfer (ESPT) across the hydrogen bond as a primary step in the relaxation dynamics.^{1–8} The fast and often barrierless ESPT process is seen to out-compete other routes to relaxation leading to stabilization, for example against dissociation in the isolated or non-hydrogen bonded molecular equivalent. Interestingly, the systems studied have often been constrained to limit broader structural changes around the hydrogen bond with structural frameworks that limit any out-of-plane motion. The AA and TFA dimers, while having planar cyclic dimer structures at equilibrium, have no such structural constraints. The carbon backbone can move and provide an alternative pathway for relaxation.

While the literature on the photodynamics of the AA and TFA dimers is limited, there are multiple studies investigating the photochemical relaxation of the acetic acid^{14–17} and TFA^{15,18} monomers upon irradiation of UV light in the gas phase. In both systems, the excitation of the lowest energy $\pi^* \leftarrow n$ transition results in photolysis and the formation of OH radicals. For the AA monomer at an excitation wavelength of 222 nm, the quantum yield for OH formation was 0.546,¹⁴ whereas in TFA at wavelengths between 200 and 220 nm, this was 0.4.¹⁸ The difference in quantum yields was speculated to be due to an increased reaction energy barrier for the formation of the OH fragment in TFA. While to the best of our knowledge, no measurements have been made of the TFA dimer, measurements performed on the AA dimer saw that the quantum yield for OH radical formation dropped significantly to 0.038, indicating that the hydrogen bonding interaction plays a significant role in the stabilization of the system against dissociation.¹⁹ Herein, we report that upon photo-excitation, we observe relaxation pathways involving structural buckling where the planarity of the initial dimer is removed. This process is seen to dominate any potential excited state proton transfer and facilitates internal conversion through conical intersections that stabilizes the dimer against dissociation and leads back to the electronic ground state on ultrafast timescales. The difference in the hydrogen bond strength of the two systems also leads to significant changes in the initial dynamics and the timescales upon which ground state recovery occurs in the AA and TFA dimers.

II. EXPERIMENTAL DETAILS

Femtosecond time-resolved infrared (TRIR) absorption experiments were performed using the ULTRA system at the Central Laser Facility (CLF). The setup has been fully described elsewhere such that we only provide brief details here.²⁰ The acid dimers were

pumped with 100 nJ of 200 nm radiation generated through sequential second harmonic and sum frequency generation processes of the 800 nm output of a Ti:sapphire laser system. The broad band mid-IR probe pulses were produced using a commercial fs-OPA (Light Conversion), resulting in a bandwidth of $\sim 400 \text{ cm}^{-1}$ in the regions measured. The resultant pump and probe pulses gave an instrument response function of $\sim 500 \text{ fs}$ full width at half maximum. An optical chopper positioned in the pump beam path blocked alternate pump pulses. This allowed for a shot-to-shot comparison of the pump-plus-probe signal with the probe-only signal. The measurements were taken at pump-probe delays between -5 and 3000 ps .

The pump and probe pulses were crossed at a small angle ($\sim 4^\circ$) through the sample cell with the polarization of the pump relative to the probe set to the “magic” angle. The beam diameters of the pump and probe through the sample were 150 and $100 \mu\text{m}$, respectively. The sample solution was pumped through a Harrick cell equipped with CaF_2 windows and $50 \mu\text{m}$ PTFE spacers. The Harrick cell was rastered in the x- and y-axes, perpendicular to the beam propagation direction, to minimize any photodamage to the sample. After passing through the sample, the probe spectrum was monitored using a 128-element mercury cadmium telluride detector (IR Associates). The spectrum was calibrated through comparison with a reference spectrum of polystyrene.

0.3M solutions of acetic acid and trifluoro-acetic acid in hexane were produced and characterized using FTIR (see Fig. 1). The hexane solvent provides a weakly interacting matrix within which the molecular dimers are formed. By using a non-polar solvent in which the dimerization constant is very large,²¹ the solution is dominated by the dimer with minimal contribution from the monomer. In the 0.3M AA solution, there is a small monomer contribution to the spectrum that can be seen around the carbonyl stretch region. The peak associated with the monomer appears at 1780 cm^{-1} and is offset from the peak in the dimer at 1718 cm^{-1} . In the equivalent region of the TFA spectrum, the monomer contribution is seen as a small wing on the peak at 1780 cm^{-1} . In both cases, the intensity of the monomer peak is over an order of magnitude lower than the dimer, which, when combined with the fact that the absorption cross section of the dimer at 200 nm is a factor of two larger than for the monomer, means that our time resolved spectra are considered clear of any monomer contributions. To test this, we performed TRIR measurements down to concentrations of 0.125M, where the dimer-to-monomer ratio is expected to be 30:1.²¹ At these concentrations, we did not observe any peaks associated with the monomer in our FTIR spectra and the dynamics measured in the TRIR were consistent with those measured at the higher concentration. The TRIR data presented have the solvent induced background subtracted from the raw data with the process for this described in Sec. I of the supplementary material.

III. COMPUTATIONAL DETAILS

A. Electronic structure calculations

In order to analyze the observed changes and assign structures in the TRIR spectrum, we have performed *ab initio* electronic structure calculations [using Molpro 2022²² for state-averaged complete active space SCF (SA-CASSCF) and Gaussian 2016 (Ver. A.03 and C.01)²³ for time-dependent density functional theory (TDDFT)] on

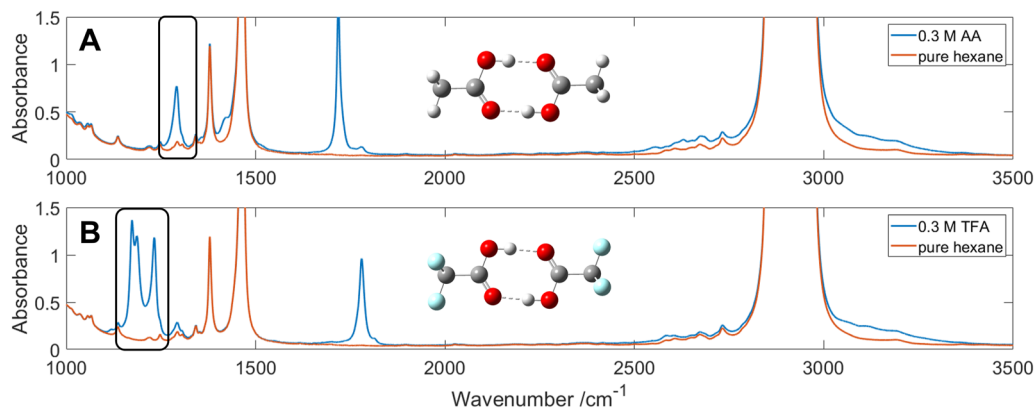


FIG. 1. FTIR spectrum of (a) 0.3M AA in hexane and (b) 0.3M TFA in hexane. In both plots, the red curve shows the pure hexane spectrum and the black box highlights the probe regions measured in the TRIR data presented in Fig. 4. In AA, the black box covers the $6B_u$ vibration, while in TFA, the black box covers the $8A_u$, $8B_u$, and $9B_u$ vibrations. More details on the assignments can be found in Sec. IV A. The insets show the equilibrium planar structure of the AA and TFA dimers in their electronic ground state.

the ground and excited state potential energy surfaces (PES) of the dimer systems. The ground state minima of the AA and TFA dimers have C_{2h} symmetry and are largely described as two monomers forming a planar backbone along the acid group, creating a double hydrogen-bonded ring. The calculations were performed on isolated dimers in the gas phase such that they ignore any contribution from the solvent. The effects of solvation on the acid dimers were explored using DFT/TDDFT and implicit solvation methods, of which the details can be found in Sec. IV of the supplementary material. The results showed that little to no interaction occurs between the solvent and the acids such that the solvent appears to act as an inert bath. The consensus is that in the scope of this study, it is sufficient to describe the acid dimers in the gas phase.

The DFT/TDDFT calculations were performed using the B3LYP functional and the 6-31+G(p,d) Pople basis set.²⁴ Lourderaj *et al.*²⁵ have demonstrated the suitability of this functional in their study of several carboxylic acid dimers (including the AA

dimer). They obtained a S_2 vertical excitation energy of 206 nm, which was in close agreement with the experimental gas-phase UV absorption maximum of 207 nm reported by Orlando and Tyndall.²⁶

Vertical excitation energies for the first four excited singlet and triplet states of both systems are provided in Table I. This table shows the results of TDDFT and ten-state SA-CASSCF(8, 10) calculations using the 6-311++G(d,p) Pople basis set (further corroboration in Sec. V A of the supplementary material). The symmetry labels given in this table highlight a disagreement between the methods used on the character of the S_3 states and above. However, these states are not accessible with the pump energies used in the present experiment, lying ~ 1 eV above the first two singlet excited states. As such, we have not investigated this point further. For both molecules, the two lowest energy triplet states, T_2 and T_1 , lie ~ 0.5 eV below the S_1 energy, are near degenerate, and lie about 1 eV lower than the rest of the triplet manifold.

TABLE I. Vertical excitation energies (eV) of the AA and TFA monomer and dimer. The values were obtained using two different methods for the first four singlet and triplet states. TDDFT uses the B3LYP functional with a 6-31+G(d,p) basis, and CAS refers to a ten-state SA-CAS-SCF(8,10), 6-311++G(d,p) basis. The symmetry labels for excitations are reported where available, and their oscillator strengths are given in parentheses.

Method	AA(eV)			TFA(eV)		
	Dimer CAS	Dimer TDDFT	Monomer TDDFT	Dimer CAS	Dimer TDDFT	Monomer TDDFT
S_1	B_g 5.97 (0.000)	B_g 5.94 (0.000)	5.78 (0.001)	B_g 5.96 (0.000)	B_g 5.71 (0.000)	5.53 (0.001)
S_2	A_u 5.99 (0.003)	A_u 6.02 (0.002)	6.86 (0.056)	A_u 5.98 (0.002)	A_u 5.79 (0.002)	7.51 (0.036)
S_3	B_u 7.75 (0.000)	A_u 6.91 (0.001)	...	A_g 6.91 (0.000)	A_u 6.69 (0.001)	...
S_4	A_g 7.91 (0.000)	B_g 6.98 (0.000)	...	B_u 7.52 (0.000)	B_g 6.76 (0.000)	...
T_1	B_g 5.57 (0.000)	B_g 5.47 (0.000)	5.22 (0.000)	B_g 5.67 (0.000)	B_g 5.21 (0.000)	4.92 (0.000)
T_2	A_u 5.59 (0.000)	A_u 5.52 (0.000)	5.88 (0.000)	A_u 5.69 (0.000)	A_u 5.26 (0.000)	5.52 (0.000)
T_3	A_u 6.46 (0.000)	A_g 5.86 (0.000)	...	A_u 7.40 (0.000)	A_g 5.50 (0.000)	...
T_4	A_g 6.47 (0.000)	B_u 5.89 (0.000)	...	B_g 7.51 (0.000)	B_u 5.53 (0.000)	...

The dimer molecular orbitals (MOs) can be largely described as the symmetrized direct sum of the monomer MO, with a slight perturbation occurring from the hydrogen bond. The S_1/T_1 and S_2/T_2 states can then be described by two $\pi^* \leftarrow n$ single excitation configurations, with the coefficients shown for AA in Table II and orbitals shown in Fig. 2. The near degeneracy of the states can be attributed to their near identical transitions. The linear combination of configurations is such that both S_1 and S_2 approximately describe excitations occurring within monomers.

Notably, the $S_0 \rightarrow S_1$ transition dipole vectors of these monomers occur out-of-plane of the carboxylic group. The formation of the dimer produces symmetrical and anti-symmetrical transition dipole combinations, resulting in an optically bright S_2 state (oscillator strength > 0) and an optically dark S_1 state (no oscillator strength). These properties are common in other hydrogen-bonded dimers and larger molecular aggregates that contain chromophores, and various methods exist to classify and quantify the state bands. In Kasha theory,²⁷ states are similarly described as linear combinations of individual monomer excited states. Coulombic intermolecular coupling is used as a means to approximate the splitting between states and explain their optical activity. The aggregates are given a label of “H” or “J” identifying which of the two states is optically dark or bright; the dimers discussed here would be classified as H-aggregates.

Nonetheless, similar carboxylic acid dimers to the ones studied here have seen recent experimental and theoretical studies, which show that the S_1 – S_2 splitting cannot be adequately approximated by pure dipole–dipole interactions. Ottiger *et al.* observed a large discrepancy in the state splitting calculated from multiple *ab initio* methods compared to experimental results (*ab initio* methods over-estimate the value by a factor of 5–25 times).^{28,29} Instead,

TABLE II. Principal configuration coefficients representing $\pi^* \leftarrow n$ orbital excitations, describing the first two singlet and triplet excited states of AA. The configuration combinations result in localized monomer excitations. The calculations were performed using SA-CASSF(8,6)/6-311++G(d,p).

Orbital/ $1B_g$ state	S_1	T_1
$\pi^* (4a_u) \leftarrow n (13b_u)$	0.5024	0.7134
$\pi^* (4b_g) \leftarrow n (13a_g)$	−0.4428	−0.6344
Orbital/ $1A_u$ state	S_2	T_2
$\pi^* (4b_g) \leftarrow n (13b_u)$	0.4828	0.6892
$\pi^* (4a_u) \leftarrow n (13a_g)$	0.4642	0.6606

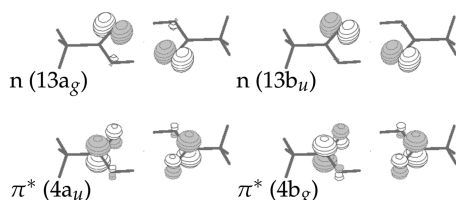


FIG. 2. Valence and symmetrized n and π^* molecular orbitals describing the principal configurations for the first two singlet and triplet excited AA dimer states are shown. The configuration coefficients are provided in Table II.

the inclusion of vibronic coupling was found necessary to provide better agreement. Thus, a non-adiabatic description of the PES is necessary to account for the state spacing, implying that population transfer between these states should be significant.

Of the ten orbitals used to evaluate the vertical excitation energies of Table I, only four HOMO and two LUMO orbitals were necessary to accurately evaluate the first two excited singlet and triplet states. Consequently, critical geometry optimizations and quasi-classical and quantum dynamic simulations were performed with this reduced active space. Furthermore, surface-hopping calculations (using the SHARC package³⁰) and quantum dynamics (using QUANTICS³¹) were done with a small 3-21G basis, which is able to qualitatively replicate the critical geometries obtained with a higher basis.

B. Quantifying the hydrogen-bond strength

To explore how fluorination and electronic excitation change the intermolecular hydrogen bonding, we have utilized several computational approaches. In the electronic ground state, we expect that the electron withdrawing nature of the fluorine atoms on TFA will have a significant weakening effect on the strength of the hydrogen bonding interaction between the two monomer components when compared with AA. To quantify the magnitude of this change, we have used the methods developed by Boxer and co-workers to calculate the effective electric field at the center of one OH bond resulting from close proximity of the other dimer component.³² The resultant electric field strength was 97 MV cm^{-1} in the AA dimer and 67 MV cm^{-1} in the TFA dimer. Both values are indicative of very strong hydrogen bonding interactions but with a significant weakening of this effect in TFA. More details of these calculations can be found in Sec. II of the supplementary material. Small structural differences also exist between the two dimers due to the electron withdrawing nature of the trifluoro-methyl group. This results in shorter bond lengths and wider bond angles in the acid moiety and a longer bond length for the C–C bond.

In the excited state, the non-equivalent nature of the two monomer components means that it is unclear how one could perform a similar analysis. In order to qualitatively inspect how the hydrogen bonding may change upon excitation of the $n\pi^*$ states, we performed two calculations that provide qualitative information on the changes in hydrogen bonding. We first look at a purely electrostatic picture and perform a partial charge analysis of the two systems in their ground and excited states to explore the electrostatic changes. We also calculate approximate interaction energies (i.e., the energy difference between the bound and separated but unrelaxed monomer components) in the ground and excited states to explore the difference in energy stabilization.

The partial charge analysis shows that upon excitation, the Mulliken charges on the hydrogen-bonded oxygen atoms decrease by 42% and 47% from -0.361 and -0.284 for AA and TFA, respectively, whereas on the hydrogen atom, this charge reduction is less than 1% in both cases. This is shown in Fig. S7 of the supplementary material and can be explained by the loss of the electron arising from the oxygen non-bonding orbital, lying in the hydrogen bond plane. This decrease in O–H charge difference implies a weakening of the hydrogen bonds upon excitation, in analogy to the electrostatic picture used for the electronic ground state, with a greater weakening of the hydrogen bond in TFA when compared with AA.

Further corroboration of the weakening of the hydrogen bonds within the acid dimers upon electronic excitation is obtained via approximate calculation of the interaction energy. The results of these calculations show a reduction in the interaction energy in the excited state, Table S2, indicating that there is less of a stabilizing interaction in the $n\pi^*$ excited states of AA and TFA than in the electronic ground state. As with the partial charge analysis, there is a greater weakening in the TFA than AA.

While we cannot quantify how much weaker the hydrogen bonding interaction is in the excited state using either of these methods, they both suggest that the hydrogen bond in the AA and TFA dimers should become weaker upon electronic excitation. Given the initially weaker interaction in TFA and that excitation appears to weaken the TFA system more than AA, one might expect TFA to be significantly less photostable than AA. More details of these calculations can be found in Sec. III of the supplementary material.

IV. RESULTS AND DISCUSSION

A. Ground state frequency analysis

The normal modes/vibrations of the two dimer systems can be largely described by symmetric/antisymmetric combinations of

monomer modes. In the context of the hydrogen-bonded ring, these result in symmetric out-of-plane (A_u) and in-plane (B_u) IR active modes and their antisymmetric dark (B_g/A_g) counterparts. The latter will become “activated” when/if the symmetry of the system is broken (as discussed in the context of the TRIR results below).

Table III provides details of the modes with significant IR intensity in the electronic ground state in the TRIR regions measured (as highlighted by the black box in Fig. 1). The vibrational modes are symmetry labeled according to the ascending rank of frequencies (starting at 1) per irreducible representation. Due to the different rank and frequency of similar vibrations in the two systems, we have performed a linear assignment using the absolute value of the overlap matrix between the TFA and AA dimer mode vectors and between the dimer and monomer vectors (the correlation between modes is typically above 0.5). This analysis allows us to qualitatively compare how the normal modes are affected by the addition of fluorine and by dimerization. The correlated monomer and dimer modes of the analogous systems are shown on the same row in Table III, with each row in this table labeled according to its relevance to the time-resolved measurements in either TFA or AA. The vector displacements associated with the dimer vibrations are also shown in Fig. 3. Similarly, modes at nearby critical geometries

TABLE III. Experimentally relevant ground state IR active modes for AA and TFA monomers and dimers are given with their symmetry, wavenumber (cm^{-1}), and relative intensities (km/mol in parentheses). All quantities have been calculated using B3LYP/6-31+G(d,p). A frequency scaling factor of 0.964 relating to the method has been applied.³³ The three TFA modes measured in the TRIR measurement are labeled as TFA1-3, with the correlated AA dimer (at higher frequencies) and monomer vibrations shown in the same row for comparison. Similarly, the AA mode tracked is given in row AA1 along with the TFA and monomer correlated modes. The mode vectors are displayed in Fig. 3.

Mode	TFA ν dimer (cm^{-1} , int.)	TFA ν monomer (cm^{-1} , int.)	AA ν dimer (cm^{-1} , int.)	AA ν monomer (cm^{-1} , int.)
TFA1	$8A_u$ 1134.8 (652.4)	$6B$ 1124.8 (313.2)	$8A_u$ 3016.5 (6.2)	$6B$ 3016.5 (3.7)
TFA2	$8B_u$ 1140.8 (561.1)	$8A$ 1153.2 (300.6)	$11B_u$ 2953.7 (3.8)	$10A$ 2953.5 (2.1)
TFA3	$9B_u$ 1185.0 (702.3)	$9A$ 1205.9 (85.9)	$13B_u$ 3066.0 (25.41)	$11A$ 3066.3 (4.2)
AA1	$10B_u$ 1292.7 (112.2)	$5A$ 635.2 (75.5)	$6B_u$ 1293.4 (370.1)	$5A$ 1162.2 (211.1)

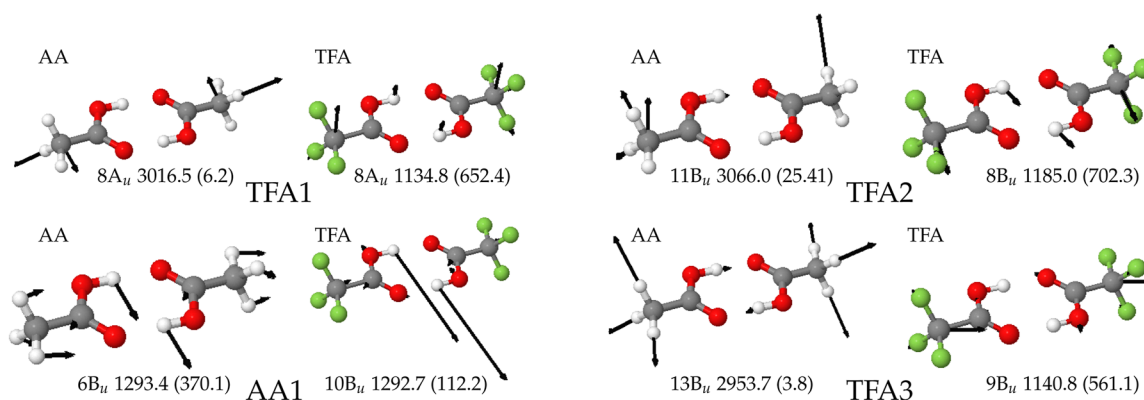


FIG. 3. Normal mode vectors of the AA and TFA dimer ground state (TDDFT) involved in the hydrogen-bond ring vibrations and relevant to the experimentally measured bands. The symmetry, wavenumbers (cm^{-1}), and relative intensities in parentheses (km/mol) are shown below each pair of correlated modes. See Table III for more details. Modes $8A_u$, $8B_u$, and $9B_u$ are measured in the TRIR for TFA. Mode $6B_u$ is measured in the TRIR for AA.

that are discussed in relation to the dynamics are referenced with their frequencies and, where possible, associated diabatically with the ground state C_{2h} frequencies.

The FTIR spectra of the AA and TFA dimer solutions are plotted in Fig. 1 along with that of the pure hexane solvent. The regions measured in the TRIR experiments described below are highlighted by the black box overlaid on the two spectra. The changes caused by fluorination mean measurements of directly comparable vibrations are not possible such that, in AA, our TRIR measurements focused on the $6B_u$ mode, around 1290 cm^{-1} , while in TFA, they focused on the $8A_u$, $8B_u$, and $9B_u$ modes around 1150 cm^{-1} . The time-dependent signals from both measurements are plotted in Fig. 4.

In the AA dimer, the displacements associated with the $6B_u$ mode are dominated by the out-of-plane motion of the hydrogen atoms associated with the hydrogen bonded ring (see Fig. 3). The $6B_u$ mode is, therefore, expected to be extremely sensitive to changes in the hydrogen bonding environment and reports directly on changes in the hydrogen bonded ring structure. The correlated mode in TFA ($10B_u$) has a significantly lower IR cross section compared to the AA $6B_u$ mode, which means directly equivalent measurements in TFA were not possible.

In the TFA dimer, we measure the $8A_u$, $8B_u$, and $9B_u$ modes, which are ostensibly related to the C–F stretch but contain a significant vector displacement of the hydrogen bonded ring (see Fig. 3). The correlated modes in the AA system ($8A_u$, $11B_u$, and $13B_u$) relate to the C–H stretch and are located at energies around 3000 cm^{-1} . This means that the equivalent AA modes strongly overlap the OH and solvent bands, making time-resolved measurements of the equivalent modes in AA impossible.

The effects of fluorination on the vibrational wavenumber and cross section of the modes sensitive to the hydrogen bonding environment mean that we have to measure different modes in the TRIR measurements of the AA and TFA dimers. While this is not ideal, the modes chosen for each system show sensitivity to the changing hydrogen bond environment and appear in the regions of the

spectrum that are free from overlapping solvent bands, producing the clear, time-dependent signals shown in Fig. 4.

B. Time-resolved measurements

The TRIR spectra collected over the first few ps of pump–probe delay are presented in Fig. 4(a) for the AA dimer and in Figs. 4(b) and 4(c) for the TFA dimer. Focusing on the AA dimer first, at early times, we observe what appear to be two excited state absorption peaks that are on either side of the ground state $6B_u$ vibrational wavenumber. The structure of the spectrum could also be explained in terms of a very broad single excited state peak overlapping with a ground state bleach signal. The excited state signal is short-lived, decaying back to the baseline within 1.5 ps with the commensurate formation of a new absorption band peaking at 1295 cm^{-1} . The peak position approximately matches the position of the ground state equilibrium structure spectrum and decays back to the baseline level within ~ 10 ps.

The appearance of new peak(s) in the spectrum at early times is indicative of an excited state absorption resulting from changes in geometry and/or bonding around the hydrogen bonded ring. The later time spectrum resembles that obtained from the un-pumped molecules with the position of the peak close to the energy expected for the ground state equilibrium geometry. This suggests that the dimer has returned to a structural configuration that is identical, or at least very similar, to that of the ground state, but with a significantly higher IR absorption cross section. At asymptotically long times, the fact that the intensity returns to the baseline suggests that all the initially excited molecules have returned to their initial equilibrium configuration with no discernible photochemical change in the ensemble within our limits of detection.

In the TFA dimer data [Fig. 4(b)], we observe very different spectral changes. In contrast to the AA dimer, there is a strong ground state bleach signal at short pump–probe delay times with TFA. This suggests that there are no similar vibrations accessible in the initially excited state or there is a significant reduction in

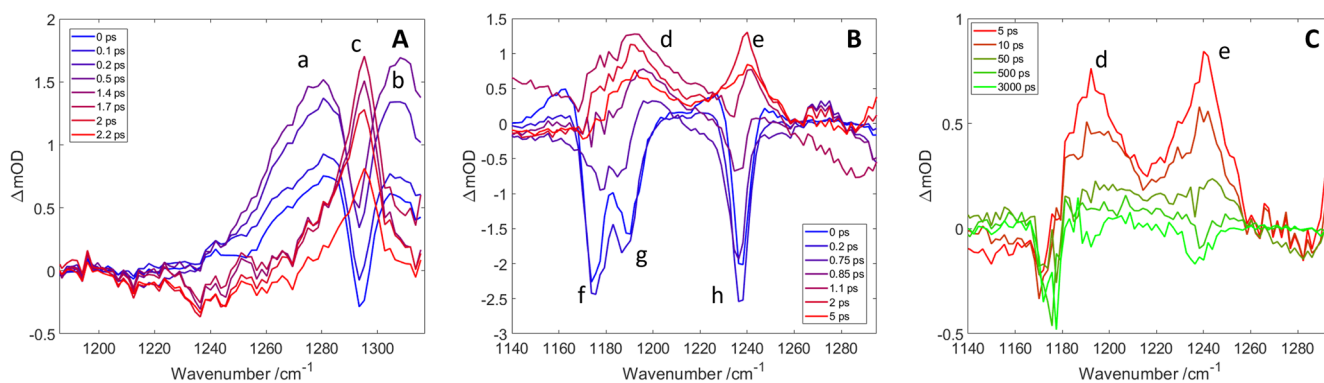


FIG. 4. TRIR spectra at a series of pump–probe delays following 200 nm excitation for AA (A) and TFA (B and C) dimers measured over the $1190\text{--}1310\text{ cm}^{-1}$ and $1140\text{--}1280\text{ cm}^{-1}$ range, respectively. For TFA, panel B shows the initial changes in the structure over the first 5 ps and panel C shows the longer-term decay of the signal and the depletion seen at ns delays. The peaks are labeled as follows: (a) S_1 $6B_u$, (b) S_1 $7A_g$, (c) S_0 $6B_u$, (d) S_1 multiple overlapping bands, (e) S_1 $9B_u$, (f) S_0 $8A_u$, (g) S_0 $8B_u$, and (h) S_0 $9B_u$.

the transition dipole of these vibrations. After ~ 1 ps, the bleach is replaced by an excited state absorption spectrum that shows a similar structure to the ground state but with peaks that are blue shifted with respect to the ground state spectrum. From this point on, the spectral shape remains constant, but the intensity decreases with an exponential time constant of ~ 100 ps (see Fig. S4 of the supplementary material). On the longest timescale measured (3 ns) [Fig. 4(c)], we observe a significant bleach signal overlapping with the ground state peak at 1178 cm^{-1} , indicating that unlike the AA dimer and on the timescale of our measurement, not all photoexcited molecules have returned to their initial configuration. This may indicate the dissociation of the TFA dimer as a consequence of the initially weaker hydrogen bonding interaction in the electronic ground state, and/or the extra weakening felt upon excitation. We note that the three peaks in the residual bleach signal show a different intensity profile than would be expected from a pure ground state depletion, suggesting that there may be some overlap with signals associated with the dissociation products.

C. Excited state potential energy landscape

To analyze the changes in the spectrum, we performed electronic structure calculations and explored the shape of the potential energy surfaces of the two dimer systems. Critical geometries and energies relevant to the discussion were obtained using 3-state SA-CASSCF(8,6)/6-311++G(d,p) methods and are shown in Figs. 5 and 6 for AA and TFA, respectively. The minima were corroborated with TDDFT (as well as other methods; see Table S8 of the supplementary material). The relevant energies obtained at critical points are provided in Table IV for AA. The critical geometries were obtained by sequential geometry optimizations that are required to

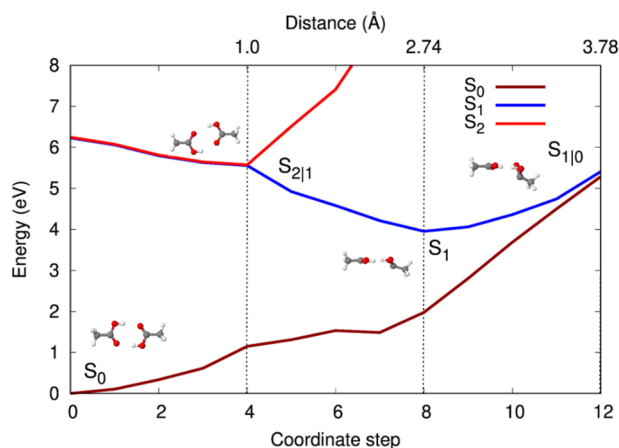


FIG. 5. SA-CAS(8,6)/6-311++G(d,p) potential energy of the first three singlet states, cut along four critical geometries of interest for the AA dimer. The values at the critical geometries are highlighted by the vertical black dashed lines. Three approximate geodesic interpolated points were used to connect these images/steps between critical geometries indexed in the lower x-axis,³⁴ while an integrated path length is shown in the top axis. The labels of the critical points are shown in the plot, as well as a small molecular diagram close by. From left to right, the positions of key structures are defined as follows: Step 0 (S_0), S_0 planar minimum; step 4 ($S_{2|1}$), S_2/S_1 skewed-planar minimum energy conical intersection (MECI); step 8 (S_1), S_1 buckled minimum; and step 12 ($S_{1|0}$), S_1/S_0 buckled MECI.

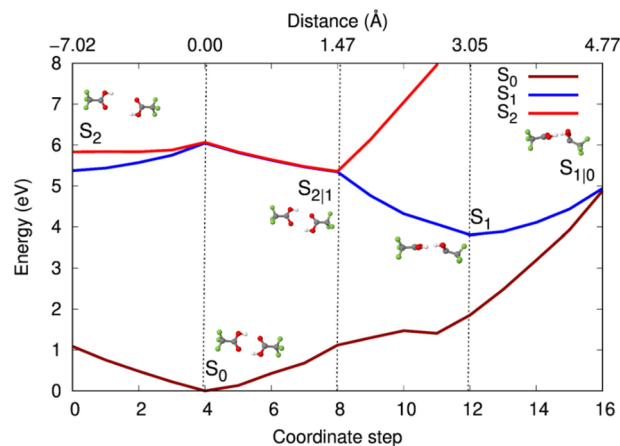


FIG. 6. SA-CAS(8,6)/6-311++G(d,p) potential energy of the first three singlet states, cut along four critical geometries of interest for the TFA dimer. The values at the critical geometries are highlighted by the vertical black dashed lines. Three approximate geodesic interpolated points were used to connect these images/steps between critical geometries indexed in the lower x-axis,³⁴ while an integrated path length is shown in the top axis (zero at the ground state reference geometry). The labels of the critical points are shown in the plot, as well as a small molecular diagram close by. From left to right, the positions of key structures are defined as follows: step 0 (S_2), S_2 dimer dissociating channel; step 4 (S_0), S_0 planar minimum; step 8 ($S_{2|1}$), S_2/S_1 skewed-planar minimum energy conical intersection (MECI); step 12 (S_1), S_1 buckled minimum; and step 16 ($S_{1|0}$), S_1/S_0 buckled MECI.

TABLE IV. AA excited state energies (eV) at the optimized critical structures relative to the ground state minimum. Minima were calculated with both CASSCF and TDDFT (basis shown in this table), while minimum energy conical intersections were calculated solely with CASSCF.

State/method	CAS(8, 6)	TDDFT/RB3LYP
Basis set	6-311++G(d,p)	6-31+G(d,p)
Minima		
AA dimer		
S_1 buckled	3.95 eV	4.82 eV
S_1 90° bent	4.03 eV	
TFA dimer		
S_1 buckled	3.81 eV	4.67 eV
S_2 twisted	6.46 eV	5.31 eV
Con. inter.		
AA dimer		
S_2/S_1 skewed-planar	5.56 eV	
S_0/S_1 buckled	5.40 eV	
TFA dimer		
S_2/S_1 skewed-planar	5.34 eV	
S_0/S_1 buckled	4.94 eV	

reach the ground state, via each state minimum and conical intersection. The calculations suggested that upon excitation to the optically bright state, S_2 , the shape of the potential energy surfaces forces both the AA and TFA dimer systems to break C_{2h} symmetry, resulting in previously dark vibrational modes becoming IR active. Figures 5 and 6 show geodesic interpolations³⁴ between the critical points important to the dynamics and plot their PES.

D. Acetic acid

Focusing on the AA system for now and with reference to the PES plotted in Fig. 5, a S_2 geometry optimization starting from the planar minimum structure of the electronic ground state leads directly into the S_2/S_1 conical intersection. The minimum energy conical intersection (MECI) ($S_{2|1}$ -CIX) was optimized and has a structure that conserves the planar symmetry, while the dimer hydrogen bond becomes slightly skewed ($S_{2|1}$ skewed-planar). An optimization of the structure in the S_1 state from the $S_{2|1}$ skewed-planar structure leads to an S_1 buckled basin where the carbonyl carbon of one of the monomers buckles out-of-plane into an sp^3 -like bonding structure, effectively pulling its methyl out of the plane. Alongside the buckling, there is an elongation of the C=O (1.23 \rightarrow 1.33 Å) bond, suggesting a weakening in the π -bonding of the carbonyl. A conical intersection search starting from the S_1 buckled geometry leads to the $S_{1|0}$ buckled intersection, ~ 1.4 eV higher in energy than the S_1 minimum. The $S_{1|0}$ buckled intersection is characterized by an even more pronounced buckling of one of the monomers, in the same manner as the S_1 buckled minimum. Optimizing in the S_0 state from the $S_{1|0}$ buckled intersection leads back to the ground state minimum. The energies of the critical points discussed here are given in Table IV. Similar structures are also seen in the monomer, where the minimization of the S_1 state also results in a buckled geometry. The asymmetric buckling and breakdown of the C_{2h} symmetry are, therefore, not unexpected as the characters of the first two excited states are monomer-localized (Table II).

We have also explored the possibility that hydrogen transfer occurs in the excited states. Potential cuts along the hydrogen transfer coordinate can be found in Fig. S12 of the supplementary material and show that there are large barriers to these processes and no potential gradients are driving the reaction along this coordinate. The potentials, therefore, suggest that the initial motions will not involve hydrogen transfer, and based on the barrier heights calculated, we suggest that these are not active in the excited states of AA dimers.

The relatively minor changes in the structure and lack of barrier on the singlet potential energy surfaces mean that the population of the S_1 buckled structure is expected to occur within ultrafast timescales. To corroborate that the “shortest” path described in the previous paragraph is the dominant pathway, we performed a modest number (14) of surface-hopping trajectories (SHARC³⁰) for a minimum of 300 fs (detailed in Sec. VI A of the supplementary material). All trajectories hopped onto the S_1 surface within the first ten femtoseconds, with one of the trajectories reaching the electronic ground state by the end of the simulation. The quick transfer to the S_1 agrees with the strong vibronic coupling observed with similar acid dimer systems.²⁹ Another minimum was also found on the S_1 surface, the 90° “buckled” dimer (S_1 90° bent), which is near degenerate to the S_1 buckled minimum (energy shown in Table IV).

The distinct changes in the structure and symmetry mean that we also expect this to show significant changes in the IR spectrum measured. For all the minimum energy structures on the PES, we calculated the normal frequencies (IR spectrum) over the experimental ranges measured, with the results provided in Table V. Vibrational frequencies have been corroborated with different electronic methods; while there is some disagreement in the precise values obtained, the structure of the spectrum is consistent between all of them (see Sec. V of the supplementary material for full details). For the stable buckled structure, there are two vibrations in the 1250–1300 cm^{-1} range measured. The symmetry breaking caused by the buckling means that the previously dark A_g modes become active, “sharing” intensity with its B_u mode partner. As an example, in Fig. 7, we provide a comparison of the spectra obtained from the S_0 planar minimum structure with that obtained from the S_1 buckled minimum structure. The spectra show the transition from a single peak in the planar structure to two peaks upon buckling. A similar exploration of the triplet-state energy critical geometries was performed, and a twisted hydrogen-bond ring T_1 minimum was found as well as a monomer buckled T_2 minimum. Quantum dynamic simulations (QUANTICS^{31,35}) were performed to estimate the extent of intersystem crossing; less than 1% of triplet state population was measured after 1 picosecond (see Sec. VI A of the supplementary material for details). The quantum dynamics and trajectory calculations, therefore, suggest that upon excitation, the dynamics will follow the path outlined in Fig. 5, with initial skewing of the hydrogen bonded ring leading to internal conversion to S_1 , whereupon the system buckles and undergoes a second internal conversion process, returning to the electronic ground state.

E. Trifluoro-acetic acid

Turning to TFA, the electronic characters of the first two excited states of TFA are analogous to that of AA. Unlike AA, however, when starting from the Franck–Condon geometry, the energy minimization of the S_2 state leads to the dissociation of the dimer, which has been corroborated with complimentary TDDFT calculations. As the S_2 state can be described as monomer localized, we expect dissociation to lead to one ground state and one excited state partner in the monomer S_1 . The optimization of the S_1 monomer

TABLE V. Wavenumbers (cm^{-1}) and intensities (km/mol in parentheses) of the normal modes monitored in the AA TRIR experiments. The labels used are based on the S_0 symmetric minimum labels with the matching of frequencies at different geometries performed as described in the text. A frequency scaling factor of 0.964 is applied for TDDFT, and a frequency scaling factor of 0.922 is applied for CASSCF.³³

Method	TDDFT	6-31+G(d,p)
State/frequency	$7A_g$	$6B_u$
S_0 planar	1280.4 (–)	1293.4 (370.1)
S_1 buckled	1305.4 (74.4)	1265.9 (225.5)
Method	CAS (8, 6)	6-311++G(d,p)
State/frequency	$7A_g$	$6B_u$
S_0 planar	1278.4 (–)	1285.2 (465.4)
S_1 buckled	1258.7 (170.0)	1284.6 (330.1)
S_1 90-buckled	1259.4 (144.5)	1274.2 (365.1)

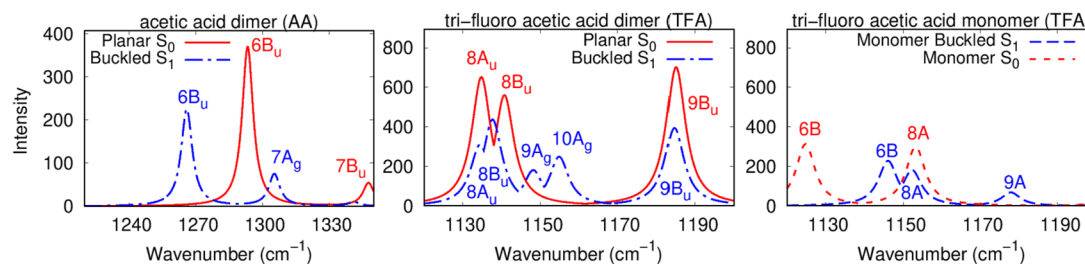


FIG. 7. Calculated IR spectra for structures associated with the planar S_0 and buckled S_1 energy minimum in the AA dimer (left), TFA dimer (middle), and TFA monomer (right). Calculated using TDDFT/B3LYP/6-31+G(d,p), with a frequency scaling factor of 0.964 applied.³³ A Lorentzian broadening of 6 cm^{-1} (full width at half maximum) is applied to all peaks. The symmetry labeling at non-symmetric geometries refers to the diabatic continuity with the modes from the ground state symmetry as explained in the text and used in the tables.

leads to a buckled structure as seen for the AA monomer (see Sec. VIII of the supplementary material for details).

We have further explored the excited state potential of the dimer system to check for other potentially stable configurations and critical structures such as those associated with conical intersections. A PES cut across these critical points is shown in Fig. 6, the critical energies are shown in Table IV, and the structures are shown in Fig. S8 of the supplementary material. We find a very similar pathway to the ground state to that of the AA dimer. The S_2/S_1 MECI was found to have a “trans” weakened hydrogen-bonded planar ring structure akin to that found in AA (S_{21} skewed-planar). From this CI, S_1 minimization leads to a S_1 minimum energy structure similar to that seen in AA with the same buckled configuration (S_1 buckled). A similar, further buckled S_1/S_0 MECI was found, $\sim 1\text{ eV}$ above the S_1 minimum (S_{10} buckled MECI). Using TDDFT, a S_2 minimum with a twisted-boat hydrogen bond ring conformation was found below the S_2 vertical excitation energy. The same structure was found $\sim 0.5\text{ eV}$ above the vertical excitation energy using CAS. The energy obtained in the CAS calculations indicates this minimum would be inaccessible at our pump energy, and, as such, we do not consider it in the rest of the discussion.

Like AA, a modest number (15) of surface hopping trajectories were performed covering the first 200–400 fs after excitation. The trajectory calculations were performed using a smaller basis set, which still qualitatively exhibits the same critical geometries. The trajectories suggest that upon excitation to the S_2 state, there is a substantial weakening of the hydrogen bond interaction, with the distance between the two monomer components increasing significantly (by $\sim 50\%$) within the first 50 fs. This is often combined with a loss in the planarity of the initial hydrogen bonded ring, further suggesting that the hydrogen bond is effectively broken. As the excited states are described by local monomer excitation, this means that as the dimer dissociates, one monomer component is in its electronic ground state, while the second is in an excited electronic state. If we consider the monomers in the dimer system formally separated (dissociated), the dimer S_1 and S_2 states become degenerate such that the monomer with the localized excitation would be in its own S_1 state, while the other would find itself in its ground state. However, during dissociation, some interaction remains such that we treat the system formally as a weakly interacting dimer. In this case, the degeneracy between the S_2 and S_1 states remains broken and we see population internally convert from the S_2 to S_1 state within the first 20 fs for all

trajectories. In some of the trajectories, population is seen to hop back and forth between the S_2 and S_1 states. Nonetheless, by the end of the simulation, the electronically excited monomer component is seen to buckle out of the plane set by the COOH functional group.

As dissociation of the TFA dimer is likely to occur, the calculated frequencies of the stable S_0 and S_1 monomer structures are shown in Table VI alongside those associated with the stable excited state structures of the dimer found in the geometry optimization procedure. For the electronically excited dimer, we find one A_u/B_g pair of modes and two A_g/B_u pairs in the frequency range covered by the experiment that share intensity as the molecule breaks symmetry.

Matching of modes at different excited state geometries with respect to the C_{2h} ground state modes was performed by linear assignment from the overlap matrix between modes. We suggest caution when interpreting the S_2 twisted TDDFT results in Table VI since the modes were only weakly correlated with those of the ground state and some unusual intensities for some of the modes were also obtained (not shown in this table). A comparison of the spectra associated with the planar ground state and S_1 -buckled dimer structures, as well as the S_1 buckled and S_0 planar structures of the monomer, are plotted in Fig. 7.

F. Discussion

In the AA dimer, the shape of the potentials suggests that, upon excitation into S_2 , the initial dynamics will lead to a lowering of the symmetry and previously IR inactive modes will become active. This change in activity can be seen in Table V, which contains the calculated normal frequencies and intensities for the critical geometries over the experimental ranges measured. The calculations suggest that initial motion will lead to a skewing of the hydrogen bonded ring as it undergoes internal conversion from the S_2 to the S_1 state and will subsequently buckle once in the S_1 state. As the initial skewing is barrierless and, therefore, expected to occur on a timescale of a few 10 s of femtoseconds, we cannot realistically expect to capture any signals associated with the initial S_2 population. The primary stable structure we expect to observe is associated with the buckled S_1 minimum.

The representative simulated IR spectra for key structures of AA are shown in Fig. 7. The spectra highlight how the change in

TABLE VI. Wavenumbers (cm^{-1}) and intensities (km/mol in parentheses) of the normal modes relevant to the TFA TRIR measurements. Both monomer and dimer wavenumbers are reported due to the potential for dissociation. The labels used are based on the S_0 symmetric minimum labels with the matching of frequencies at different geometries performed as described in the text. Note that the g and u subscripts are only relevant to the dimer. The TDDFT, TFA twisted minimum exhibits some unusual intensities and frequencies, so the aforementioned linear assignment was skipped and the frequencies are merely presented in ascending order. A frequency scaling factor of 0.964 has been applied to the TDDFT calculations, and a scaling factor of 0.922 has been applied to the CASSCF calculations.³³

State/Freq.	$8A_u$	$7B_g$	$8B_u$	$9A_g$	$9B_u$	$10A_g$
Method	TDDFT 6-31+G(d,p)					
S_0 planar dimer	1134.8 (652.4)	1131.0 (–)	1140.8 (561.1)	1150.9 (–)	1185.0 (702.3)	1183.4 (–)
S_0 planar monomer	N/A	1124.8 (313.2)	N/A	1153.3 (300.6)	N/A	1205.9 (85.9)
S_1 buckled dimer	1134.5 (310.6)	1057.9 (383.8)	1137.7 (438.1)	1148.3 (181.8)	1184.7 (394.4)	1155.0 (249.4)
S_1 buckled monomer	N/A	1074.8 (293.4)	N/A	1146.1 (228.5)	N/A	1177.9 (68.6)
S_2 twisted dimer	1119.2 (1122.4)	1120.6 (170.5)	1159.3 (605.9)	1159.4 (99.9)	1232.7 (7.2)	1251.3 (78.9)
Method	CAS(8,6) 6-311++G(d,p)					
S_0 planar dimer	1183.7 (767.2)	1184.5 (–)	1246.3 (742.4)	1243.7 (–)	1267.0 (742.3)	1274.9 (–)
S_1 buckled dimer	1103.0 (158.1)	1175.8 (341.3)	1246.5 (382.3)	1226.6 (375.4)	1258.7 (629.4)	1269.5 (160.9)
S_2 twisted dimer	1211.0 (444.8)	1404.7 (123.7)	1258.2 (414.9)	1252.3 (223.8)	1271.9 (369.6)	1292.8 (320.4)

symmetry associated with the buckling process leads to a significant change in the IR activity and cross section. Around 1300 cm^{-1} , there are two vibrational modes associated with the ring that have B_u and A_g symmetries, respectively. In the electronic ground state, the highly symmetric planar structure means that only the B_u vibration is IR active such that the spectrum consists of a single intense peak. As the dimer buckles and the symmetry is reduced, intensity is shared between the two vibrations and the (formally labeled) B_u and A_g vibrations are now both IR active. The appearance of two peaks is seen across all electronic states (both singlet and triplet) that show a buckled or twisted structure. While this change from one to two peaks is common to all levels of theory, the frequency and shift relative to the peak observed in the electronic ground state are less consistent. The rapid formation of the two peaks in the experimental spectrum, occurring on an ultrafast timescale combined with the dynamics calculations, strongly indicates that the buckled structure is formed in the S_1 electronic state after internal conversion. We, therefore, assign the two peaks seen in the early time experimental spectrum to the $6B_u$ and $7A_g$ modes in the S_1 electronic state. We note that while the absolute energies of the calculated and measured peaks differ, the spacing and shifts appear consistent. The differences in energy between the two peaks seen in the experimental and theoretical spectra are very similar, with a peak to peak separation of the broad experimental peaks of $\sim 35\text{ cm}^{-1}$, compared to $\sim 40\text{ cm}^{-1}$ in the theoretical spectrum.

The subsequent decay of the double peak structure indicates the reformation of the highly symmetric planar structure within 2 ps. According to our calculations, the only electronic state that shows a planar equilibrium structure is the electronic ground state. We, therefore, assign the appearance of the single peak at 1295 cm^{-1} to a vibrationally hot ground state dimer that has been formed following internal conversion through the buckled conical intersection between the S_1 and S_0 electronic states. We find the large positive signal and that the frequency is so similar to that of the vibrational ground state surprising but cannot find another plausible explanation for this. A tentative explanation for the appearance of the

signal is as follows: the positive intensity of the 1295 cm^{-1} signal is indicative of a hot band transition of $n \rightarrow n + 1$, since the transition strength increases as \sqrt{n} . The bright B_u/A_u modes seen in the ground state spectra have a symmetric PES. A fit of the PES cut along these shows a “squeezing” of the PES (purely positive, even monomial term fits) as the energy increases toward that of the S_1/S_0 MECI. Assuming uncoupled harmonic motion holds at such energies, the spectra would be expected to shift slightly to the blue for these modes (see Sec. X of the supplementary material for the PES and HO eigenvalues).

The decay of the signal over the course of the next 10 ps is consistent with vibrational cooling and reformation of the ground vibrational state of the dimer. Assuming similar rates of vibrational cooling in the electronically excited states, we suggest that, given the picosecond lifetime of the S_1 state, there is limited time to cool and trap any significant excited state population in the S_1 minimum despite the appearance of a reasonable barrier to the S_1/S_0 conical intersection. We also note that due to the lack of dynamical correlation in the CAS wavefunction, the S_{110} MECI energy may be overestimated, which, when combined with the fact that vibronic coupling can facilitate internal conversion in the vicinity of the MECI (and not exactly at that point), could lead to an effective reduction in the barrier to the MECI. The AA dimer, therefore, shows ultrafast internal conversion dynamics with rapid reformation of the electronic ground state facilitated by gross-structural changes centered around the hydrogen-bonded ring.

The spectral changes in the TFA dimer suggest that significantly different dynamics are at play. As dissociation of the dimer could play a significant role in the dynamics, we plot the calculated spectra for the TFA monomer and dimer in the ground and electronically excited states over the experimentally measured range in Fig. 7. The initial bleach signal seen in the experiment indicates that the spectrum has undergone a significant change in the structure (Fig. 4); theory suggests that upon excitation, the dimer will dissociate. The much lower absorption cross section associated with the monomers fits well with the observed bleach such that we take this signal as

a marker of an effective breaking of the hydrogen bonds between the monomer TFA components. The excited state absorption spectrum seen experimentally after ~ 1 ps has a similar structure to that of the dimer but with a slight blue shift and increased intensity in the $1190\text{--}1230\text{ cm}^{-1}$ range, between the main peaks seen in the ground state spectrum. This aligns well with the predicted spectrum associated with the buckled S_1 geometry of the dimer. The extended lifetime suggests that internal conversion back to the ground state is much slower than in the AA dimer. The extended excited state lifetime could indicate that the triplet states become important in TFA. We do not see any spectral changes to suggest this, but as the accessible triplet states are expected to show similarly buckled structures, then there may not be any spectral change expected when comparing the T_1 and S_1 buckled structures. The decay of the signal, therefore, gives an effective excited state lifetime of ~ 100 ps.

The experimental observations and theoretical calculations, therefore, provide the following picture of the photodynamics of the TFA dimer. The excitation at 200 nm leads to the population of the S_2 excited state. The dynamics on the excited state surface lead to an increased distance between the two TFA monomer components, effectively breaking the hydrogen bonding interaction. As excitation into S_2 is effectively a monomer localized excitation, this leads to one TFA component forming in the electronic ground state and one in an electronically excited state. The accessible monomer excited states, S_2 and S_1 , are degenerate and lead to buckling of the monomer TFA backbone. The solvent cage effectively traps the two monomer fragments and stops complete separation such that the majority of the monomers undergo geminate recombination on a picosecond timescale. Considering that the dimer S_1 (buckled) state can be described as a small perturbation of the monomer states, recombination is likely possible, while the buckled monomer remains in its S_1 state. The non-radiative relaxation pathway and timescales of the TFA monomer were beyond the scope of this study, but any buckled monomer undergoing relaxation down to the ground state could also naturally recombine. The 100 ps lifetime of the S_1 buckled signal suggests that access to the S_1/S_0 conical intersection is hindered, leading to an extended excited state lifetime. The extended lifetime could be due to the trapping of population at the S_1 minimum caused by vibrational energy transfer to the solvent, and/or intramolecular vibrational energy redistribution, caused by the dissociation and recombination process. Both mechanisms would lead to less energy in the modes required for buckling and accessing the S_1/S_0 conical intersection. We observe no clear signature that we can directly associate with internal conversion to the electronic ground state such that it is likely that the 100 ps lifetime relates to internal conversion and vibrational cooling. Finally, we note that a residual bleach signal is apparent in the spectrum at our longest delays measured. The ratio of the early to late time bleach signals suggests that $\sim 10\%$ of the excited state population does not reform the ground state dimer on the 3 ns timescale measured. We suggest that this is the proportion of excited molecules that do not undergo geminate recombination and remain as monomers within the sample measured, or further photo-degrade releasing hydroxyl radicals. We note that the position of the monomer vibrational peaks plotted in Fig. 7 would overlap with peaks g and h in the experimental spectrum shown in Fig. 4. This could explain why peak f shows a higher level of depletion than peaks g and h in the bleach signal seen at long delays.

V. SUMMARY

In summary, we have measured the UV-induced photochemistry of AA and TFA dimers in the solution phase using TRIR spectroscopy and analyzed these through comparison with *ab initio* calculations. The combination of experiment and theory allows us to correlate spectral changes with the structural dynamics of the dimer systems.

The analysis of the measurements suggests that in the AA dimer, the hydrogen bond is sufficiently strong that it stabilizes against dissociation. The dimer, therefore, undergoes an ultrafast IC process and the formation of a buckled intermediate in the S_1 electronically excited state. In AA, the formation of the buckled structure occurs on a sub-50 fs timescale according to trajectory calculations, which means that we cannot resolve this transition experimentally. The subsequent relaxation into the electronic ground state is also ultrafast, and the planar equilibrium structure is reformed within a couple of picoseconds. In contrast, the fluorination in TFA weakens the hydrogen-bonding interaction enough that in the excited state, it cannot stabilize against dissociation. The ground state bleach observed shows this dissociation into two TFA-monomers, one in the electronic ground state and the other in an electronically excited state. The monomer fragment in the excited state buckles and then recombines with the ground state monomer fragment, leading to a recovery of the bleach signal and the appearance of an excited state absorption. The subsequent buckled dimer S_1 signal appears much longer lived, with an apparent lifetime of 100 ps, which suggests a slow conversion back to a hot ground state molecule. A residual ground state bleach suggests that not all excited molecules return back to their ground electronic state.

The results presented highlight several new facets of how hydrogen bonding interactions affect photochemical processes. In the AA dimer, the very strong hydrogen bonding interaction effectively stabilizes the system against dissociation. Relaxation is not through hydrogen or proton transfer but through a gross structural change (buckling on one monomer component backbone) that maintains the hydrogen bond plane. We are unaware of any previous examples where such structural changes have been observed. In TFA, the significantly weaker but still very strong, hydrogen bond is no longer effective in stabilizing against dissociation. The weakening on the hydrogen bond by fluorination means that the system dissociates. We suggest that, in the gas phase, this would lead to a complete separation of the two monomers and that recombination is facilitated here by the caging effects of the surrounding solvent environment. Upon recombination, however, the dynamics of the system resemble that of the AA dimer system, with a buckled structure facilitating ground state recovery.

The comparison between AA and TFA also opens up intriguing questions about the impact of the different hydrogen bond strengths on photochemical stability and dynamics. The weaker hydrogen bond strength in the TFA system leads to reduced photochemical stability and a breaking of the hydrogen bonding interaction holding the two molecules together. The extended excited state lifetime observed upon recombination also suggests that access to relaxation pathways back to the electronic ground state is also affected by the hydrogen bond strength and the photochemical pathway taken. While we cannot draw general conclusions from these two systems alone, the observations correlate well with the predictions given by

our simple analysis of the changes in the hydrogen bond strength. The ability to measure a range of AA dimers with a controlled range of hydrogen bond strengths through further chemical substitution will allow us to explore this effect in more detail in future experiments.

SUPPLEMENTARY MATERIAL

The details of the data treatment and the removal of solvent background are presented, alongside theoretical details and supporting calculations.

ACKNOWLEDGMENTS

The authors acknowledge the STFC for access to the ULTRA facility. R.S.M. and E.P. acknowledge the Royal Society for a studentship and research support (Grant No. RGF/EA/180111), and R.S.M. acknowledges the Royal Society for a University Research Fellowship (Grant Nos. UF100047 and UF150655). M.J.P. acknowledges the EPSRC for funding through Grant Nos. EP/T021675 and EP/V006746 and the Leverhulme Trust (Grant No. RPG-2020-208). R.A.I. and H.M.G. acknowledge the EPSRC for a studentship (Grant Nos. EP/N509577/1 and EP/T517793/1). For the purpose of open access, the author has applied a Creative Commons Attribution (CC BY) license to any author accepted manuscript version arising.

AUTHOR DECLARATIONS

Conflict of Interest

The authors have no conflicts to disclose.

Author Contributions

E. Plackett: Data curation (equal); Formal analysis (lead); Writing – original draft (supporting); Writing – review & editing (equal). **C. Robertson:** Data curation (equal); Formal analysis (equal); Writing – original draft (supporting); Writing – review & editing (equal). **A. De Matos Loja:** Data curation (equal); Formal analysis (equal); Writing – original draft (supporting); Writing – review & editing (equal). **H. McGhee:** Data curation (equal); Writing – review & editing (equal). **G. Karras:** Data curation (equal); Project administration (supporting); Resources (equal). **I. V. Sazanovich:** Data curation (equal); Project administration (supporting); Resources (equal). **R. A. Ingle:** Data curation (equal); Writing – review & editing (equal). **M. J. Paterson:** Funding acquisition (equal); Supervision (equal); Writing – review & editing (equal). **Russell S. Minns:** Conceptualization (lead); Funding acquisition (equal); Project administration (lead); Supervision (equal); Writing – original draft (lead).

DATA AVAILABILITY

The data that support the findings of this study are available from the corresponding author upon reasonable request.

REFERENCES

- 1 E. Samoylova, W. Radloff, H. H. Ritze, and T. Schultz, *J. Phys. Chem. A* **113**, 8195 (2009).
- 2 H. Böhnke, J. Bahrenburg, X. Ma, K. Röttger, C. Näther, M. F. Rode, A. L. Sobolewski, and F. Temps, *Phys. Chem. Chem. Phys.* **20**, 2646 (2018).
- 3 D. LeGourriérec, V. A. Kharlanov, R. G. Brown, and W. Rettig, *J. Photochem. Photobiol., A* **130**, 101 (2000).
- 4 M. Sliwa, N. Mouton, C. Ruckebusch, L. Poisson, A. Idrissi, S. Aloïse, L. Potier, J. Dubois, O. Poizat, and G. Buntinx, *Photochem. Photobiol. Sci.* **9**, 661 (2010).
- 5 N. Mataga and Y. Kaifu, *J. Chem. Phys.* **36**, 2804 (1962).
- 6 P. Zhou and K. Han, *Acc. Chem. Res.* **51**, 1681 (2018).
- 7 D. A. Horke, H. M. Watts, A. D. Smith, E. Jager, E. Springate, O. Alexander, C. Cacho, R. T. Chapman, and R. S. Minns, *Phys. Rev. Lett.* **117**, 163002 (2016).
- 8 K. Röttger, H. J. Marroux, M. P. Grubb, P. M. Coulter, H. Böhnke, A. S. Henderson, M. C. Galan, F. Temps, A. J. Orr-Ewing, and G. M. Roberts, *Angew. Chem., Int. Ed.* **54**, 14719 (2015).
- 9 B. Marchetti, T. N. V. Karsili, M. N. R. Ashfold, and W. Domcke, *Phys. Chem. Chem. Phys.* **18**, 20007 (2016).
- 10 C. Fang, R. R. Frontiera, R. Tran, and R. A. Mathies, *Nature* **462**, 200 (2009).
- 11 R. K. Venkatraman, S. Kayal, A. Barak, A. J. Orr-Ewing, and S. Umaphathy, *J. Phys. Chem. Lett.* **9**, 1642 (2018).
- 12 M. Marazzi, S. Mai, D. Roca-Sanjuán, M. G. Delcey, R. Lindh, L. González, and A. Monari, *J. Phys. Chem. Lett.* **7**, 622 (2016).
- 13 P. Song and F.-C. Ma, *Int. Rev. Phys. Chem.* **32**, 589 (2013).
- 14 D. L. Singleton, G. Paraskevopoulos, and R. S. Irwin, *J. Am. Chem. Soc.* **111**, 5248 (1989).
- 15 H. T. Kwon, S. K. Shin, S. K. Kim, H. L. Kim, and C. R. Park, *J. Phys. Chem. A* **105**, 6775–6779 (2001).
- 16 S. S. Hunnicutt, L. D. Waits, and J. A. Guest, *J. Phys. Chem.* **93**, 5188 (1989).
- 17 S. S. Hunnicutt, L. D. Waits, and J. A. Guest, *J. Phys. Chem.* **95**, 562 (1991).
- 18 M. C. Osborne, G. Li, and I. W. Smith, *Phys. Chem. Chem. Phys.* **1**, 1447 (1999).
- 19 D. L. Singleton, G. Paraskevopoulos, and R. S. Irwin, *J. Phys. Chem.* **94**, 695 (1990).
- 20 G. M. Greetham, P. Burgos, Q. Cao, I. P. Clark, P. S. Codd, R. C. Farrow, M. W. George, M. Kogitmtz, P. Matousek, A. W. Parker, M. R. Pollard, D. A. Robinson, Z.-J. Xin, and M. Towrie, *Appl. Spectrosc.* **64**, 1311 (2010).
- 21 Y. Fujii, H. Yamada, and M. Mizuta, *J. Phys. Chem.* **92**, 6768 (1988).
- 22 H.-J. Werner, P. J. Knowles, G. Knizia, F. R. Manby, and M. Schütz, *WIREs Comput. Mol. Sci.* **2**, 242 (2012).
- 23 M. J. Frisch, G. W. Trucks, H. B. Schlegel, G. E. Scuseria, and M. A. Robb, *Gaussian16 Revision C.01*, Gaussian Inc, Wallingford, CT, 2016.
- 24 M. J. Frisch, J. A. Pople, and J. S. Binkley, *J. Chem. Phys.* **80**, 3265 (1984).
- 25 U. Lourderaj, K. Giri, and N. Sathyamurthy, *J. Phys. Chem. A* **110**, 2709 (2006).
- 26 J. J. Orlando and G. S. Tyndall, *J. Photochem. Photobiol., A* **157**, 161 (2003).
- 27 N. J. Hestand and F. C. Spano, *Chem. Rev.* **118**, 7069 (2018).
- 28 P. Ottiger, S. Leutwyler, and H. Köppel, *J. Chem. Phys.* **136**, 174308 (2012).
- 29 P. Ottiger, H. Köppel, and S. Leutwyler, *Chem. Sci.* **6**, 6059 (2015).
- 30 S. Mai, M. Richter, M. Heindl, M. F. S. J. Menger, A. Atkins, M. Ruckebauer, F. Plasser, L. M. Ibele, S. Kropf, M. Oettel, P. Marquetand, and L. Gonzalez, Sharc2.1: Surface hopping including arbitrary couplings—Program package for non-adiabatic dynamics, sharc-md.org (2019).
- 31 G. A. Worth, K. Giri, G. W. Richings, I. Burghardt, M. H. Beck, A. Jäckle, and H.-D. Meyer, Quantics University of Birmingham, Birmingham, UK, version 1.1.
- 32 S. D. Fried and S. G. Boxer, *Acc. Chem. Res.* **48**, 998 (2015).
- 33 Computational chemistry comparison and benchmark database (CCCBDB): Precomputed vibrational scaling factors, <https://cccbdb.nist.gov/vibscalejust.asp>, (2022).
- 34 S. Smidstrup, A. Pedersen, K. Stokbro, and H. Jónsson, *J. Chem. Phys.* **140**, 214106 (2014).
- 35 G. Richings, C. Robertson, and S. Habershon, *Faraday Discuss.* **216**, 476 (2019).